Title: Forecasting Gamma-ray Bursts using Gravitational Waves

Abstract

We explore the intriguing possibility of employing future gravitational-wave interferometers to detect the inspiral of compact binaries early enough to alert the electromagnetic observatories so that a gamma-ray burst (GRB) can be observed in its entirety from its very start. We quantify the ability to predict a GRB by computing the time a canonical binary neutron star (BNS) system takes to inspiral from a certain threshold frequency to its final merger. We define this threshold frequency to be the gravitational-wave frequency at which the RMS-averaged strain due to the BNS system accumulates a signal-to-noise (SNR) ratio of 15. For our computation of advance warning times, we consider BNS systems at luminosity distances of (i) $D \lesssim 200\,$Mpc in a three-interferometer network with Advance LIGO's design sensitivity and (ii) $D \lesssim 1000\,$Mpc in a similar network, but with the Einstein Telescope's B configuration sensitivity. We find in the case of that Advanced LIGO we may get a few minutes of warning time if we get lucky whereas the Einstein Telescope will provide us with warning times as long as a few hours.

We also consider binary black hole neutron star systems with the hopes of observing a tidal disruption event in the future. However, our findings indicate that witnessing such an event will be very unlikely even after the Einstein Telescope becomes operational.

Introduction

We reserve the symbol f to denote the GW frequency of the dominant quadrupole mode, which is twice the orbital frequency f_K. Relatedly, we define the following angular frequencies: $\omega = 2\pi f, \Omega = 2\pi f_K$ with $\omega = 2\Omega$. We employ the $\simeq$ symbol for quantities which we can compute exactly, but list finite digits and $\approx$ for quantities whose values we know approximately. Overdots denote time derivative with respect to detector time, e.g., $\dot{E} = dE/dt$.

Mention **KAGRA** [2, 3], starts 2018-2019, design at 2021-2022, 152Mpc range (K. Somiya, ET-meeting at Birmingham, 2017)

Cosmic Explorer [5], LIGO India, Australia China(?)

Ref. [32] already attemps some forecast, but they focus on the search algorithm side of things

We also disreagrd the fact that GRBs are collimated and will most often not point toward the Earth. Ref. [4] looks at this? (CHECK)

Binary systems composed of neutron stars

Newtonian evolution of BNS

For us, the starting point for the evolution of a binary under the emission of GWs is the expression for the power generated given by

$$\dot{E} = \frac{G}{5c^5} \langle \dddot{Q}_{ij} \dddot{Q}_{ij} \rangle \,. \tag{1}$$

This is the celebrated Einstein quadrupole formula. Here, Q_{ij} is a trace-reversed mass quadrupole moment which is the dominant contribution to the power generated by a system with changing mass moments.

Here, we are specifically interested in the motion of two point masses in bound motion around a common center of mass. Labelling the masses by $m_1 \leq m_2$, we have, for a binary in a circular orbit with Keplerian angular frequency Ω and separation $2r$,

$$\dot{E} = \frac{32}{5} \frac{G\mu^2}{c^5} r^4 \Omega^6 \tag{2}$$

where $\mu = m_1 m_2/M$ is the reduced mass and $M = m_1 + m_2$ is the total mass. We justify our simplification of motion to circular orbits in Sec. 4.3.

An important quantity in GW astronomy is the chirp mass of the binary given by

$$M_c = \mu^{3/5} M^{2/5} = \frac{(m_1 m_2)^{3/5}}{(m_1 + m_2)^{1/5}} \,, \tag{3}$$

which turns Eq. (2) into

$$\dot{E} = \frac{32}{5}\frac{c^5}{G}\left(\frac{GM_c\,\omega}{2c^3}\right)^{10/3}, \tag{4}$$

where, recall $\omega = 2\Omega$ is the angular frequency of the quadrupolar GWs. The quantity in parantheses in Eq. (4) is ubiquitous in post-Newtonian theory and is referred to as the dimensionless inverse separation x. As $x \sim v^2/c^2$, it is used to keep track of post-Newtonian orders and we can from in Eq. (4) that $\dot{E} \sim x^5$.

The energy generated by the acceleration of the masses is radiated away in GWs, which makes the total energy of the binary more negative, i.e., the orbit becomes more bound. Since the total energy is given by

$$E_b = -\frac{Gm_1m_2}{2r}\,. \tag{5}$$

$\dot{E}_b < 0$ implies the orbital radius must decrease in time. Using Kepler's third law, $\Omega^2 = GMr^{-3}$ and Eq. (3) we obtain

$$E_b = -\left(\frac{G^2M_c^5\omega^2}{32}\right)^{1/3}, \tag{6}$$

Energy conservation dictates that $\dot{E} = -\dot{E}_b$. Using the chain rule to determine $\dot{E}_b$ from Eq. (6) and setting the resulting expression equal to Eq. (4) yields $\dot{\omega}$ as a function of ω and various constants. Translating this expression using $\omega = 2\pi f$ we arrive at the standard expression for the GW frequency evolution

$$\dot{f} = \frac{96}{5}\pi^{8/3}\frac{(GM_c)^{5/3}}{c^5}f^{11/3} \tag{7}$$

This can be integrated straightforwardly after defining a new time variable $\tau \equiv t_{\text{coal}} - t$ that equals zero when the neutron stars coalesce. We can now define an inspiral time at a given GW frequency

$$\tau_{\text{insp}}(f) = \frac{5}{256\pi}\frac{c^5}{(\pi GM_c)^{5/3}}f^{-8/3}, \tag{8}$$

which we can rewrite as follows

$$\tau_{\text{insp}}(f) \simeq 2.18\,\text{s}\left(\frac{1.21M_\odot}{M_c}\right)^{5/3}\left(\frac{100\,\text{Hz}}{f}\right)^{8/3}, \tag{9}$$

where $1.21M_\odot$ is the chirp mass corresponding to $m_1 = m_2 = 1.4M_\odot$.

We can also compute the number of GW cycles over the course of an inspiral. Given that the orbital period $T(t)$ varies over a much larger time scale than T itself we can write

$$\mathcal{N}_{\text{cyc}}(f) = \int_f^{f_{\text{max}}}\frac{f}{\dot{f}}\,df = \frac{1}{32\pi}\frac{c^5}{(\pi GM_c)^{5/3}}\left[f^{-5/3} - f_{\text{max}}^{-5/3}\right] \tag{10}$$

We now introduce a cut-off for the inspiral imposed by the frequency of the innermost stable circular (ISCO) orbit in Schwarzschild spacetime

$$\Omega_{\text{ISCO}} = \frac{c^3}{6^{3/2}GM}. \tag{11}$$

We will see in Sec. 4.3 that $f_{\text{ISCO}} \sim \mathcal{O}(1000)\,\text{Hz}$ for a system with $M \approx 2M_\odot$. Moreover, the frequencies of interest for our advance warning time estimations will be $\lesssim \mathcal{O}(10)\,\text{Hz}$ meaning that $f^{-5/3} \gg f_{\text{ISCO}}^{-5/3}$. Therefore, at the leading (Newtonian) order, the number of GW cycles can be approximated by

$$\mathcal{N}_{\text{cyc}}(f) \simeq \frac{1}{32\pi}\frac{c^5}{(\pi GM_c)^{5/3}}f^{-5/3}\,. \tag{12}$$

Restoring some familiar numbers in this expression yields

$$\mathcal{N}_{\rm cyc}(f) \simeq 1.6\times 10^4 \left(\frac{10\,{\rm Hz}}{f}\right)^{5/3} \left(\frac{1.21 M_\odot}{M_c}\right)^{5/3} . \tag{13}$$

This expression is quite telling: if a ground-based interferometer picks up an inspiralling BNS at $f = 10\,{\rm Hz}$ then there will be $\gtrsim \mathcal{O}(10^4)$ GW cycles in the detector's data stream until the merger.

Another useful relation is how the inspiral time scales with respect to the orbital radius corresponding to the observed GW frequency. From Kepler's third law, we immediately have $\dot{r}/r = -2\dot{\Omega}/(3\Omega) = -2\dot{f}/(3f)$, which, via Eq. (8), yields $\dot{r}/r = -1/(4\tau)$ which integrates to

$$r(\tau) = r_i \left(\frac{\tau}{\tau_i}\right)^{1/4} , \tag{14}$$

where $r_i, \tau_i = t_{\rm coal} - t_i$ are the initial radius and time that the BNS is "picked up" by a detector. Solving $\tau(f_i) = \tau_i$ for $f_i = \Omega_i/\pi$ using Eq. (8) and rewriting Ω_i as a function of r_i via Kepler's third law gives us

$$\tau_i = \frac{5}{256}\,\frac{c^5 r_i^4}{G^3 M^2 \mu} \simeq 9.829\times 10^6\,{\rm yrs} \left(\frac{T}{1\,{\rm hr}}\right)^{8/3} \left(\frac{M_\odot}{M}\right)^{2/3} \left(\frac{M_\odot}{\mu}\right) . \tag{15}$$

Let us now turn our attention to the GWs generated by the inspiral. The GWs themselves actually are tensor distortions $h_{\mu\nu}$ of the flat Minkowski spacetime propagating at the speed of light. In more technical terms, they satisfy $\Box h_{\mu\nu} = 0$, i.e., the flat spacetime sourceless wave equation meaning that we are considering the solutions far from the GW source, in the so-called wave zone defined by the condition $c/f \ll D$. In a suitable gauge, such as the commonly used TT (transverse-traceless) gauge, it can be shown that there exist only two physical degrees of freedom which manifest themselves as two independent polarization amplitudes h_+ and $h_\times$. For a circular binary at a distance D these states read

$$h_+(t) = \frac{4}{D}\left(\frac{GM_c}{c^2}\right)^{5/3} \left(\frac{\pi f(t)}{c}\right)^{2/3} \left(\frac{1+\cos^2\iota}{2}\right) \cos[\Phi_{\rm N}(t)], \tag{16}$$

$$h_\times(t) = \frac{4}{D}\left(\frac{GM_c}{c^2}\right)^{5/3} \left(\frac{\pi f(t)}{c}\right)^{2/3} \cos\iota \sin[\Phi_{\rm N}(t)], \tag{17}$$

where $\iota = \cos^{-1}(\hat{\mathbf{n}}\cdot\hat{\mathbf{L}})$ is the inclination angle between the line of sight unit vector $\hat{\mathbf{n}}$ and the orbital angular momentum unit vector $\hat{\mathbf{L}}$. E.g., for an orbit seen edge on, $\iota = \pi/2$ which is actually the case of a purely plus-polarized wave, $h_\times = \cos(\pi/2) = 0$. When $\iota = 0$ the orbit is seen face-on and we have a circularly-polarized wave: $\langle h_+\rangle = \langle h_\times\rangle$ where $\langle\ldots\rangle$ denote time-averages over one orbit. Note that as f increases in time, so does $h(t)$ hence the characteristic "chirping" of GW signals.

$\Phi_{\rm N}(t)$ in Eqs. (16, 17) is the phase of the GWs given by

$$\begin{aligned}\Phi_{\rm N}(t) &= \int_{t_i}^{t} dt'\omega(t') \\ &= -2\left(\frac{5GM_c}{c^3}\right)^{-5/8} (t_{\rm coal}-t)^{5/8} + \Phi_0 \,.\end{aligned} \tag{18}$$

$\Phi_0 \equiv \Phi(t = t_{\rm coal})$ is an integration constant. The subscript N denotes the Newtonian (leading-order) contribution. Higher-order contributions can be added in terms a post-Newtonian series which make up $\lesssim 2\%$ of the total phase. Although we will include contributions up to and including 2PN to obtain the results of Sec. 6, we will not explicitly show these expressions which can be found in Ref. [12].

The nomenclature "plus" $(+)$ and "cross" $(\times)$ follows from the effects that passing GWs have on the plane transverse to their direction of propagation. If we were to conceive of an imaginary detector made up of a circular configuration of point-particles lying in the x-y plane, a GW propagating along the z direction would stretch/compress the circular arrangement in a $+$ and $\times$ pattern which is the manifestation of the tidal strain of the GWs on the tranverse plane. Next, let us briefly explore how a real detector, i.e., an interferometer, responds to passing GWs.

Interferometer response to gravitational waves

LIGO-Virgo configuration: L-shaped topology

We start by first considering the L-shaped interferometer topology dating back to Michelson. Although the GWs are described by propagating tensor modes, an interferometer (IFO) can only measure a scalar quantity known as the response function (or GW strain) which is a linear combination of the polarizations given by

$$h(t) = F_+(\theta,\phi,\psi)\, h_+(t) + F_\times(\theta,\phi,\psi)\, h_\times(t), \tag{19}$$

where

$$F_+ = \frac{1}{2}\left(1+\cos^2\theta\right)\cos 2\phi\cos 2\psi - \cos\theta\sin 2\phi\sin 2\psi, \tag{20}$$

$$F_\times = \frac{1}{2}\left(1+\cos^2\theta\right)\cos 2\phi\sin 2\psi + \cos\theta\sin 2\phi\cos 2\psi \tag{21}$$

are the antenna pattern functions of the detectors; θ,ϕ are the sky coordinates; and ψ is an additional angle coming from the respective rotations of detectors' frames to source frame. We can't apriori know θ,ϕ,ψ. However, we can extract their values with some limited precision over the course of an inspiral (preferably of BNS) emitting GWs which sweep across the detection band of more than one interferometer over thousands of cycles. This was indeed the case of GW170817 with a source sky localization of $28\,\mathrm{deg}^2$ using data from three inteferometers [8]. For our estimations, we will use suitable averages of these angles. For details on how to obtain Eqs. (20, 21) see, e.g., Sec. 4.2.1 of Ref. [14].

To compute the advance warning times we will need to know how "loud" the binaries become as they sweep across the interferometers' band. This is achieved by computing the signal-to-noise ratio (SNR) of the GWs in the detectors' data stream. This is done in the frequency domain so we need the Fourier transforms of the time-domain strains of Eqs. (16) and (17)

$$\tilde{h}_+(f) = A\,\frac{c}{D}\left(\frac{GM_c}{c^3}\right)^{5/6} e^{i\Psi_+(f)}\,\frac{1}{f^{7/6}}\,\frac{1+\cos^2\iota}{2}, \tag{22}$$

$$\tilde{h}_\times(f) = A\,\frac{c}{D}\left(\frac{GM_c}{c^3}\right)^{5/6} e^{i\Psi_\times(f)}\,\frac{1}{f^{7/6}}\,\cos\iota, \tag{23}$$

where $A = \pi^{-2/3}\sqrt{5/24}$. Explicit expressions for $\Psi_{+,\times}$ show that they are out of phase by $\pi/2$ (the details of the Fourier transformation can be found in Sec. 4.5 of Ref. [11]). Accordingly, the Fourier transform of the detector strain (19) is given by

$$\tilde{h}(f) = A\,\frac{c}{D}\left(\frac{GM_c}{c^3}\right)^{5/6} f^{-7/6}\, e^{i\Psi_{\rm N}}\, Q(\theta,\phi,\psi,\iota), \tag{24}$$

where

$$Q(\theta,\phi,\psi,\iota) = F_+(\theta,\phi,\psi)\frac{1+\cos^2\iota}{2} + iF_\times(\theta,\phi,\psi)\cos\iota, \tag{25}$$

is the quality factor. The i in front of $F_\times$ in $Q(\theta,\phi,\psi,\iota)$ is due to the $\pi/2$ phase difference between $+$ and $\times$ modes. $\Psi_{\rm N}$ is the leading-order contribution to the frequency-domain phase

$$\Psi_{\rm N} = \Psi_+(f)|_{\rm N} = 2\pi f(t_{\rm coal} + D/c) - \Phi_0 - \frac{\pi}{4} + \frac{3}{128}\left(\pi f\,\frac{GM_c}{c^3}\right)^{-5/3}. \tag{26}$$

Higher-order contributions up to and including 3.5PN can be found in Ref. [14].

The detection criterion we will employ here is quantified in terms of the optimal signal-to-noise ratio (SNR) defined by

$$\rho = \left[\int_0^\infty d\ln f\,\frac{|2\tilde{h}(f)\sqrt{f}|^2}{S_n(f)}\right]^{1/2}, \tag{27}$$

where $\sqrt{S_n(f)}$ is the *amplitude spectral density* (ASD) [also called spectral strain sensitivity] of the detector. It is usually this quantity that is shown in a typical interferometer strain sensitivity plot with the characteristic strain, $\tilde{h}_c(f) \equiv 2\tilde{h}(f)\sqrt{f}$, due to various GW sources overlaid for comparison. We will show such plots in Sec. 6.

Substituting Eq. (24) into Eq. (27) yields

$$\rho^2 = \frac{5}{6}\pi^{-4/3}\frac{c^2}{D^2}\left(\frac{GM_c}{c^3}\right)^{5/3}|Q(\theta,\phi,\psi,\iota)|^2\int_0^{f_{\rm ISCO}} df\,\frac{f^{-7/3}}{S_n(f)}\,, \tag{28}$$

where we truncate the integral at the cut-off frequency of the inspiral $f_{\rm ISCO} = \Omega_{\rm ISCO}/\pi$.

It remains to compute $|Q(\theta,\phi,\psi,\iota)|^2$. Since we can not know the direction of the source a priori, it is appropriate to average over the angles θ,ϕ,ψ,ι which we compute via the following RMS-averaging integral

$$\langle F_+^2\rangle \equiv \frac{1}{2\pi}\int_0^{2\pi} d\psi\,\frac{1}{4\pi}\int_0^{2\pi} d\phi\int_0^{\pi} d\theta\sin\theta\,F_+^2(\theta,\phi,\psi) = \frac{1}{5} \tag{29}$$

and likewise $\langle F_\times^2\rangle = 1/5$. Finally, we average over the orbital inclination angle

$$\frac{1}{2}\int_0^{\pi} d\iota\sin\iota\left[\left(\frac{1+\cos^2\iota}{2}\right)^2 + \cos^2\iota\right] = \frac{4}{5}. \tag{30}$$

Thus we have that

$$\langle|Q(\theta,\phi,\psi,\iota)|^2\rangle_{\theta,\phi,\psi,\iota} = \frac{4}{25}. \tag{31}$$

As we will also consider the case of $\psi = 0, \iota = 0$, we additionally introduce the following θ,ϕ-only averages

$$\langle F_+^2\rangle_{\theta,\phi} = \frac{7}{30}, \qquad \langle F_\times^2\rangle_{\theta,\phi} = \frac{1}{6} \tag{32}$$

yielding

$$\langle|Q(\theta,\phi,\psi=0,\iota=0)|^2\rangle_{\theta,\phi} = \frac{2}{5}. \tag{33}$$

Finally, we add the case of an optimally-oriented, purely $+$-polarized source ($\psi = 0, \iota = 0$) that is directly overhead ($\theta = 0$) simply resulting in

$$\langle|Q(\theta=0,\phi=0,\psi=0,\iota=0)|^2\rangle = 1. \tag{34}$$

In a network of N interferometers, we can define a total effective SNR as follows

$$\rho_{\rm tot} = \left[\sum_{i=1}^{N}\rho_i^2\right]^{1/2} \tag{35}$$

where Eq. (28) is employed to compute ρ_i coming from individual interferometers each with a specific quality factor Q_i. Here, instead of working with specific quality factors of the LIGO and the Virgo interferometers, we consider an *imaginary network* of three detectors ($N = 3$), where one interferometer is optimally oriented/positioned, another one operates at the RMS average thus its sensitivity is relatively suppressed by a factor $2/5$ (Eq. 31) due to suboptimal configuration. Our third detector has even lower sensitivity with a relative suppression factor of $4/5 - \sqrt{2/5} \simeq 0.1675$ which is essentially a $\{\theta\text{-}\phi\}$-RMS away from the overall RMS averaged value of 2/5. This is our way of simulating a future detection in the Advanced-LIGO-Virgo network of 2020s where the three interferometers will yield varying SNRs due to their differing quality factors. Therefore, to represent our multi-interferometer network, we introduce the norm of the frequency-domain strain (24) for each interferometer

$$\tilde{H}_i(f) \equiv \tilde{A}_i\,h_0\,f^{-7/6}, \tag{36}$$

where

$$h_0 = \frac{c}{D}\left(\frac{GM_c}{c^3}\right)^{5/6} \tag{37}$$

and the $\tilde{A}_i$ are given in Table 1. The SNR for each interferometer can now be written as

$$\rho_i = 2\tilde{A}_i\, h_0 \left[\int_0^{f_{\rm ISCO}} df\, \frac{f^{-7/3}}{S_{\rm n}(f)}\right]^{1/2}. \tag{38}$$

We arbitrarily make the following assignments for our network: $h = 1, m = 2, l = 3$ representing high, medium, low strains/SNRs, respectively. We summarize our network in the following Table 1.

IFO (i)	configuration	$\tilde{A}_i$	$\tilde{H}_i(f)$
1	high (h)	A	$Ah_0\, f^{-7/6}$
2	medium (m)	$\frac{2}{5}A$	$\frac{2}{5}Ah_0\, f^{-7/6}$
3	low (l)	$\left(\frac{4}{5} - \sqrt{\frac{2}{5}}\right) A$	$\left(\frac{4}{5} - \sqrt{\frac{2}{5}}\right) Ah_0\, f^{-7/6}$

Table 1: Our imaginary network of three L-shaped interferometers (IFOs). Column four lists the magnitude of the strain for each IFO via Eq. (36). "Configuration" describes how ideally oriented/positioned an IFO is with respect to a compact binary source. High means ideal configuration maximizing Q_i. Medium is the RMS-averaged response. Recall $A = \pi^{-2/3}\sqrt{5/24}$.

We can now write the total SNR for our network

$$\rho_{\rm tot} = \sqrt{\rho_h^2 + \rho_m^2 + \rho_l^2}. \tag{39}$$

We will start Sec. 6 by testing our network with GW170817 whose signal got picked up by the LIGO detectors around $f = 30\,$Hz. So we will change the lower limit of the integral in Eq. (39) from 0 to 30. For our advance warning times we will further use separate initial frequencies for each inteferometer as we will explain in Sec. 6.

Einstein Telescope configuration: triangular topology

Current design of Einstein Telescope is based on a [equilateral] triangular configuration with 10 km arm-lengths [35]. Within this equilateral triangle, ET will consist of three V-shaped cryogenic interferometers housed underground to sigificantly reduce seismic and gravity-gradient noises [35]. This closed topology will allow the detector to form a null stream completely devoid of a signal [36], which can be used to rule out spurious events [37]. As we will show below, the response function and the quality factor of the triangular configuration are independent of the azimuthal angle ϕ hence ET will have no blind spots [1]. However, the 60° arm separation reduces the strain of a V-shaped interferometer by a factor of $\sin 60^\circ = \sqrt{3}/2$ compared to an L-shaped interferometer. So for a single V-IFO the antenna patterns of (20, 21) become

$$F_+^1(\theta,\phi,\psi) = \frac{\sqrt{3}}{2}F_+(\theta,\phi,\psi), \qquad F_\times^1(\theta,\phi,\psi) = \frac{\sqrt{3}}{2}F_\times(\theta,\phi,\psi)\,, \tag{40}$$

where the superscript 1 labels one of the three V's of the triangle. Since the other two V IFOs lie in the same plane as the first one, their antenna patterns can be obtained simply by rotating in the azimuthal direction by $120^\circ, 240^\circ$, respectively

$$F_{+,\times}^2(\theta,\phi,\psi) = F_{+,\times}^1(\theta,\phi + 2\pi/3,\psi), \tag{41}$$
$$F_{+,\times}^3(\theta,\phi,\psi) = F_{+,\times}^1(\theta,\phi - 2\pi/3,\psi). \tag{42}$$

The invidual antenna responses combine to cancel the ϕ and ψ dependence of the combined power pattern

$$F_{\triangle}^{2} \equiv \sum_{A=1}^{3} \left(F_{+}^{A}\right)^{2} + \left(F_{\times}^{A}\right)^{2} = \frac{9}{32}\left(1 + 6\cos^{2}\theta + \cos^{4}\theta\right). \tag{43}$$

From this, we immediately have that the RMS average is given by $\langle F_{\triangle}\rangle = 3/\sqrt{10}$ and the minium value is $F_{\triangle}(\pi/2) = 3/\sqrt{32}$; thus a triangular detector made-up of three V-IFOs has all-sky coverage.

For the total SNR accumulated in a triangular detector we have

$$\begin{aligned}\rho_{\text{tot},\triangle}^{2} &= \sum_{A=1}^{3} \rho_{A}^{2} \\ &= \frac{5}{6}\,\pi^{-4/3}\frac{c^{2}}{D^{2}}\left(\frac{GM_{c}}{c^{3}}\right)^{5/3} |Q(\theta,\phi,\psi,\iota)|_{\triangle}^{2} \int_{0}^{f_{\text{ISCO}}} df\, \frac{f^{-7/3}}{S_{n}(f)}\,, \end{aligned} \tag{44}$$

where

$$|Q(\theta,\phi,\psi,\iota)|_{\triangle}^{2} = \sum_{A=1}^{3} \left(F_{+}^{A}\right)^{2} \frac{1+\cos^{2}\iota}{2} + \left(F_{\times}^{A}\right)^{2} \cos\iota \tag{45}$$

which is independent of ϕ [1]. We once again take the RMS average of this quantity

$$\bar{Q}_{\triangle}^{2} \equiv \langle |Q(\theta,\phi,\psi,\iota)|_{\triangle}^{2}\rangle_{\theta,\phi,\psi,\iota} = \frac{9}{25} \tag{46}$$

which is $5/2$ times higher than a single L-shaped IFO's RMS average of 4/25 [cf. Eq. (31)].

As we can not know the source sky position or orientation we will use the RMS-averaged SNR for our computations

$$\rho_{\text{tot},\triangle} = \frac{36}{25} A^{2} h_{0}^{2} \int_{0}^{f_{\text{ISCO}}} df\, \frac{f^{-7/3}}{S_{n}(f)}, \tag{47}$$

where h_0 is given by Eq. (37) and $A = \pi^{-2/3}\sqrt{5/24}$ as before. Accordingly, we define an RMS-averaged frequency-domain strain

$$\begin{aligned}\tilde{H}_{\triangle}(f,D) &\equiv A\,\bar{Q}_{\triangle}\,h_{0} f^{-7/6} \\ &= \frac{1}{2}\sqrt{\frac{3}{10}}\,\frac{c}{D}\left(\frac{GM_{c}}{c^{3}}\right)^{5/6} f^{-7/6}. \end{aligned} \tag{48}$$

It is this strain that we will use as a typical ET source; thus in this sense, $\tilde{H}_{\triangle}(f,D)$ is like the $\tilde{H}_{i}(f)$ of Table 1. But whereas in the case of a three L-IFO network we represented the detector response due to a single source in terms of three different values $\tilde{H}_{i}(f)$, for ET we will only consider $\tilde{H}_{\triangle}(f)$ as we have already angle-averaged over all three V-IFOs antenna patterns. In Sec. 6.0.2 we will consider BNS systems inspiralling at varying luminosity distances as typical sources for ET. To compute the resulting SNRs, we will slightly modify Eq. (47) and use $\sqrt{S_{n}(f)}$ for the B and C configurations of ET.

Before we present our results, we list the various idealizations/simplifications that we adopt to simplify our computations. For each idealization we present an estimated error. Our overall conclusion is that our simplifications do not significantly change our estimations of the advance warning times.

Simplifications and idealizations used in evolving the inspiral

In this section, we justify our simplifications with brief computations.

1. *Neglecting strong-field gravity and finite-size effects.* As our aim here is to provide a rough estimation for the advance warning times, we will model the neutron stars using point masses and carry out this treatment all the way to the merger. The point-particle treatment is severely inadequate for the strong-field evolution of the binary. However, these systems spend only roughly the last second of the inspiral in this regime, therefore our underestimation of the strong-field effects will

not matter for timescales lasting dozens of minutes to hours. For example, from $f = 100\,\mathrm{Hz}$, the inspiral lasts a mere ≈ 2.18 seconds until merger. The canonical BNS above has separation $r \approx 155.5\,\mathrm{km}$ at $f = 100\,\mathrm{Hz}$, which translates to a dimensionless strength of gravity of $\approx 2.66\%$ for which the Newtonian evolution is adequate. We will nonetheless supplement our Newtonian (leading order) evolution with post-Newtonian (pN) knowledge up to second post-Newtonian order (2pN). Though it is now possible to go up to 4pN, we suffice with 2pN here as higher-order contributions make miniscule changes to our estimations for advance warning times.

2. *Truncating the inspiral at the Schwarzschild ISCO.* We artificially end the inspirals at the Schwarzschild ISCO of the BNS with coordinate radius $r_{\text{ISCO}} = 6M$ and angular frequency $\Omega_{\text{ISCO}} = (M/r_{\text{ISCO}}^3)^{1/2}$ in natural units, which translates to the following dominant-mode (quadrupole) GW frequency
$$f_{\text{ISCO}} = \frac{c^3}{6^{3/2}\pi G M} \simeq 1571\,\mathrm{Hz}, \tag{49}$$
where $M \equiv m_1 + m_2 = 2.8 M_\odot$. The true ISCO is located at $r < r_{\text{ISCO}}$, however, there is no simple expression for it. Additionally, above $f \approx 200\,\mathrm{Hz}$ tidal effects are expected to show up in the GW signal. A faithful evaluation of BNS systems above $f \gtrsim 100\,\mathrm{Hz}$ is a very active branch of general relativity today, but beyond the scope of this article. As we showed above, our disregard for relativistic effects costs us a few seconds at most.

3. *Setting $m_1 = m_2 = 1.4M_\odot$.* Let us also briefly explore what the cost of setting $m_1 = m_2 = 1.4M_\odot$ will be for our calculations. Including the error bars, the known range for neutron star masses runs from $\sim 0.5M_\odot$ to $\sim 3M_\odot$ with the actual values restricted between $\sim 1M_\odot$ and $\sim 2M_\odot$ [6] (one exception being J1748-2021B with mass $2.74^{+0.21}_{-0.21} M_\odot$ [7]). Of these measured masses, a subset comprised of double neutron stars, such as the famed Hulse-Taylor binary, have the smallest error bars with masses ranging from $\sim 1.2M_\odot$ to $\sim 1.5M_\odot$. Additionally, the masses involved in GW170817 are inferred to be between $1.17M_\odot$ and $1.60M_\odot$ [8]. Therefore, let us restrict the masses to lie between $1.2M_\odot$ and $1.6M_\odot$ then focus on the quantities of interest for us, which are the inspiral time (τ_{insp}), the GW strain at the detector in the frequency domain ($\tilde{h}$) and the frequency of the innermost stable circular orbit (f_{ISCO}) given by Eq. (49) above. From the previous section, we know how these scale in terms M_c, M thus m_1, m_2, all of which we summarize in Table 2 below.

Quantity	Standard Scaling	Scaling in terms of m_1, m_2	Min $\leq$ Value$_{1.4}$ $\leq$ Max
τ_{insp}	$M_c^{-5/3}$	$(m_1 m_2)^{-1}(m_1+m_2)^{-1}$	$0.335 \leq 0.5 \leq 0.794$
$\tilde{h}$	$M_c^{5/6}$	$(m_1 m_2)(m_1+m_2)^{3/2}$	$0.7834 \leq 0.891 \leq 0.996$
f_{ISCO}	M^{-1}	$(m_1+m_2)^{-1}$	$0.4375 \leq 0.5 \leq 0.583$

Table 2: The scaling of the physical quantities of interest in this article in terms the binary masses m_1, m_2 restricted to lie between $1.2M_\odot$ and $1.6M_\odot$. We used Kepler's third law to obtain $f \sim f_K \sim M^{1/2}$. Value$_{1.4}$ represents the value of the quantities in column three evaluated at $m_1 = m_2 = 1.4M_\odot$. Unlike the orbital frequency f_K, the ISCO frequency f_{ISCO} scales as M^{-1} as shown in Eq. (49).

The ranges in column four show that $\tilde{h}$ changes roughly by $\pm 10\%$ across our chosen NS mass range whereas the variation in f_{ISCO} matters not as it affects the advance warning times by less than second (see above). The inspiral time seems to be more sensitive to our chosen mass values as indicated by roughly the $^{+60\%}_{-30\%}$ variation in Table 2. As our intent is to provide an estimation for advance warning times in terms of orders of magnitude, this variation is tolerable.

4. *Neglecting eccentricity.* We further simplify our treatment by considering only quasi-circular inspirals meaning that at any given instant, the orbit can be treated as a circular orbit with constant

Keplerian frequency $f_K = (GM/r^3)^{1/2}/(2\pi)$, where r is the radius of the circular orbit. It was Peters & Matthews who first showed that eccentric binaries circularize in the weak field [9]. Using $\dot{a} = \dot{a}(a, e), \dot{e} = \dot{e}(a, e)$ they obtained

$$a(e) = c_0 \frac{e^{12/19}}{1-e^2} \left(1 + \frac{121}{304} e^2\right)^{870/2299} \equiv c_0\, g(e) \;, \tag{50}$$

where a is the semi-major axis of the eccentric orbit and c_0 is a constant. Thus, for $e \ll 1$ we have $g(e) \approx e^{12/19}$, which means that for a system with current parameters a_i, e_i, we can write $e \approx [a\, g(e_i)/a_i]^{19/12}$. Let us apply this to determine the eccentricity of the Hulse-Taylor binary pulsar when it will have $f = 2f_K = 1\,\mathrm{Hz}$, i.e., $a \simeq 810.5\,\mathrm{km}$ with currently observed parameters of $a_i \simeq 2 \times 10^6\,\mathrm{km}$ and $e_i \simeq 0.617$. A quick calculation yields $e \simeq 1.09 \times 10^{-10}$. Hence, we see that the BNS orbits will have circularized by the time they enter the interferometers' bandwidth.

5. *Quasi-circularity.* Next, let us test the assumption that the motion is quasi-circular. This implies that that the timescale for the orbital radius to change is much longer than the orbital timescale, i.e., radial velocity $\ll$ tangential velocity during the inspiral. From $\Omega^2 = GMr^{-3}$ we can straightforwardly obtain an expression for the ratio of radial velocity to tangential velocity

$$\frac{|\dot{r}|}{r\Omega} = \frac{2}{3} \frac{|\dot{\Omega}|}{\Omega^2}. \tag{51}$$

The quasi-circular approximation implies that $|\dot{r}| \ll r\Omega$ which translates to $|\dot{\Omega}| \ll \Omega^2$ which then gives

$$\frac{\dot{\Omega}}{\Omega^2} = \frac{96}{5} \frac{(GM_c)}{c^5}^{5/3} \Omega^{5/3} \ll 1 \tag{52}$$

using Eq. (7). For example, setting $\dot{\Omega}/\Omega^2 = 10^{-3}$ yields $f = \Omega/\pi \simeq 142.8\,\mathrm{Hz}$ which, as explained above, is practically the last second before the merger. Thus, we see that we can safely employ the quasi-circular motion assumption in our estimations for advance warning times.

6. *Neglecting higher-order multipole moments.* Another reasonable question is how much our estimation of advance warning times is affected by neglecting higher-order contributions to the loss of energy coming from, e.g., the current quadrupole and the mass octupole moments. It can be shown that the power radiated by the current quadrupole ($\dot{E}_{\mathrm{cq}}$) by a binary in a circular orbit is $\mathcal{O}(v^2/c^2)$ smaller than the dominant quadrupole power. More precisely, we have [11]

$$\frac{\dot{E}_{\mathrm{cur}}}{\dot{E}} = \frac{1215}{896} \frac{v^2}{c^2} \left(\frac{m_2 - m_1}{M}\right)^2 = \frac{1215}{896} \frac{(\pi GMf)^{2/3}}{c^2} \left(\frac{m_2 - m_1}{M}\right)^2 . \tag{53}$$

At $f = 100\,\mathrm{Hz}$, the first two factors $\simeq 3.6 \times 10^{-2}$ for $M = 2.8 M_\odot$ which tells us that even in the strong-field regime, the next-to-leading order contribution is a two orders of magnitude smaller. The ratio in Eq. (53) is further supressed by $(m_2 - m_1)/M^2$ which, for our idealized equal-mass system, yields zero so we can neglect the current-quadrupole radiation completely. In a similar fashion, it can be shown that the power radiated by the mass octupole ($\ell = 3$) scales the same way as in Eq. (53) with respect to the dominant mass quadrupole radiation, but is ~ 50 times smaller. Hence we can neglect it without worry for our work. Higher moments are suppressed by higher factors of v^2/c^2 as can be shown using post-Newtonian theory. Thus, our exclusiveness to keeping only the mass-quadrupole radiation is well justified.

7. *Neglecting the neutron star spins.* It is generally believed that NSs do not have large enough angular momentum to impart interesting spin effects into the GWs emitted by the BNS systems. The dominant effect due to the spins is the spin-orbit (SO) precession which contributes to the energy flux at the 1.5pN order [$\mathcal{O}(v^3/c^3)$] with respect to the leading-order quadrupole $\dot{E}$ of Eq. (2) [12]. Restricting to the case of $m_1 = m_2$ we obtain

$$\frac{\dot{E}_{\mathrm{SO}}}{\dot{E}} \lesssim 4 \frac{G\Omega m}{c^3} \chi + \mathcal{O}\left(\frac{v^5}{c^5}\right) , \tag{54}$$

where we introduced the dimensionless Kerr spin parameter $\chi \equiv S/(Gm^2)$ which, for a NS with spin S, can be written as

$$\chi = \frac{c}{G}\frac{I}{m^2}\frac{2\pi}{P}, \tag{55}$$

where m is the mass, P is the spin period, and $I = (2/5)mR^2\kappa$ is the moment of inertia of the NS with R being the radius of the NS and $\kappa \approx \mathcal{O}(1)$ an intrinsic constant (see, e.g., Sec. 6.2 of [10]). A rather compact NS with $m = 1.4M_\odot, R = 11\,\text{km}, P = 10\,\text{ms}$ has $\chi \lesssim 0.05$ whereas the fastest spinning known NS has $\chi \lesssim 0.04$ [13]. Therefore, at $f = 100\,\text{Hz}$, the first term in the RHS of Eq. (54) gives 4.252×10^{-4}. On the other hand, the spin-spin effects contribute at $\mathcal{O}(v^4/c^4) \times \dot{E}$ hence $\lesssim \dot{E}_{\text{SO}}$. Thus, we have justified our negligence of the effects of NS spins.

8. *Neglecting cosmological effects.* When we take into account the effects of the large-scale structure of the universe, many quantities of interest are scaled by $(1+z)^\alpha$ where α is the appropriate power. The standard treatment adopts a Friedmann-Robertson-Walker cosmology with scale factor $a(t)$ and curvature $k = \pm 1$, or 0. Introducing the subscript $_s$ to denote quantities evaluated at the source frame, we have the following cosmological corrections

$$D \rightarrow (1+z)a(t)D, \tag{56}$$

$$f \rightarrow (1+z)^{-1} f_s\,. \tag{57}$$

Given that $\dot{f}_s \sim f_s^{11/3}, h(t) \sim D^{-1} f_s^{2/3}$, the observed frequency evolution and the GW strain change according to

$$\dot{f} \ \sim (1+z)^{5/3} f^{11/3}, \tag{58}$$

$$h(t) \sim (1+z)^{5/3} h(t). \tag{59}$$

Looking at Eqs. (7, 16, 17) we spot a common factor of $M_c^{5/3}$ in all of them. Therefore, we can accommodate the cosmological effects by introducing the redshifted chirp mass $\mathcal{M}_c \equiv (1+z)M_c$ which changes Eqs. (7, 16, 17) to

$$\dot{f} = \frac{96}{5}\pi^{8/3}\frac{(G\mathcal{M}_c)^{5/3}}{c^3} f^{11/3}, \tag{60}$$

$$h_c(t) = \frac{4}{D}\left(\frac{G\mathcal{M}_c}{c^2}\right)^{5/3}\left(\frac{\pi f}{c}\right)^{2/3}, \tag{61}$$

where f is the usual frequency in the observer/detector frame. So we see that the effects of the cosmological redshifting can be accounted for by the transformation $M_c \rightarrow \mathcal{M}_c$. This is because both $\dot{f}$ and the GW amplitude are governed by the time scale GM_c/c^3. For our work here, the only important consequence is the redshifting of the frequency at which we truncate the inspiral, i.e., $f_{\text{ISCO}} \simeq 1571\,\text{Hz}$ in the source frame. For our work, we consider a maximum BNS distance of 1 Gpc which is reasonable given the sensitivity of A-LIGO and the ET. $D = 1\,\text{Gpc}$ translates to $z \approx 0.25$. Therefore, in the detector frame f_{ISCO} is redshifted to $f \approx 1257\,\text{Hz}$. From our computations above, we know that this shift adds a negligible correction to the timescales that interest us here. Thus we may safely disregard the effects cosmology.

GW170817 as a test of our model Advanced LIGO-Virgo network

On 17 August 2017, at 12:41:04 UTC, GWs from the inspiral and merger of a binary neutron star system were detected by the Advanced LIGO-Virgo network. The event, first picked up by LIGO Hanford (H1), swept from $\sim 30\,\text{Hz}$ to $\sim 2000\,\text{Hz}$ in the detectors' frequency band with an accumulated total SNR of $\rho_{\text{tot}} = 32.4$ [8] The inferred duration of the event in the network bandwidth is ~ 60 seconds during which ~ 3000 cycles of GW were emitted [15]. Assuming low-spin priors ($\chi \leq 0.05$, see point 7 of Sec. 4.3), the following values were inferred for the total mass, the chirp mass, and the luminosity distance of the source with 90% confidence:

$$M = 2.74^{0.04}_{-0.01} M_\odot, M_c = 1.188^{+0.004}_{-0.002} M_\odot, D = 40^{+8}_{-14}\,\text{Mpc}. \tag{62}$$

Note that the error bar for the chirp mass is very small due to the fact that it can be extracted to high precision over thousands of GW cycles via Eq. (7).

How well does the "naive" formulation based on the quadrupole formula perform? To test this, let us first compute the inspiral time, τ_{insp}, and the number of GW cycles, $\mathcal{N}_{\text{cyc}}$, for this BNS system with initial frequency $f_i = 30\,\text{Hz}$ and final frequency $f_{\text{ISCO}} \simeq 1605.37\,\text{Hz}$. Eqs. (8) and (12) provide us with the leading-order values

$$\tau^{\text{0PN}}_{\text{insp}} \simeq 55.91\,\text{seconds}, \quad \mathcal{N}^{\text{0PN}}_{\text{cyc}} \simeq 2680\,. \tag{63}$$

If we wish to do better, we can add all of the known post-Newtonian contributions (up to 3.5PN[1]) resulting in

$$\tau^{\text{3.5PN}}_{\text{insp}} \simeq 56.65\,\text{seconds}, \quad \mathcal{N}^{\text{3.5PN}}_{\text{cyc}} \simeq 2711\,. \tag{64}$$

These are very close to the inferred values of $\tau_{\text{insp}} \approx 60$ seconds and $\mathcal{N}_{\text{cyc}} \approx 3000$ which we can obtain if we use $f_i \approx 28 - 29\,\text{Hz}$.

We now test our imaginary network using the best-inferred values for M, M_c, D from GW170817 given in Eq.(62) above and neglecting the cosmological corrections as 40 Mpc is in our "local" neighbourhood when considering cosmological distances. The test involves computing the SNRs $\rho_i, i = h, m, l$ via a slightly modified version of Eq. (38)

$$\bar{\rho}_i \equiv \rho_i(f_0, f_f) = 2\tilde{A}_i\, h_0 \left[\int_{f_0}^{f_f} df\, \frac{f^{-7/3}}{S_{\text{n}}(f)}\right]^{1/2}. \tag{65}$$

where $f_0 = 30\,\text{Hz}, f_f = f_{\text{ISCO}}$ for GW170817 and $\tilde{A}_i$ given in Table 1. For $S_{\text{n}}(f)$ we use actual [noise-subtracted] L1 data for GW170817 from LIGO's website [18]. The data, sampled at 4096 Hz, is given as a discrete time series $h(t_i)$ for a duration of 2048 seconds in time steps of $\Delta t = 1/4096 \simeq 2.44 \times 10^{-4}$ seconds. We first Fourier-transform this data to frequency space and apply several high- and low-frequency filters to isolate a window of $f \in [10, f_{\text{ISCO}}]$. The LIGO Open Science Center has a detailed Python-based tutorial on how to do this using the data from the very first GW detection (GW150914) [19]. We use a `Mathematica` based code developed at UCD to do the same for GW170817.

Fig. 1 shows our network. The red curve is L1's ASD (sensitivity) during GW170817. We assume our three IFOs to identically have this sensitivity, but because their orientations and response functions differ, their sensitivity to a localized source is reduced. We represent this reduction by lowering the amplitude of the incoming GWs by appropriate factors explained in Sec. 3 and shown in Table 1. The amplitude-adjusted strains $\tilde{H}_i(f)$ are represented by the solid ($i = h$), dashed ($i = m$), and dotted ($i = l$) lines in the figure where we actually plot $2\sqrt{f}\tilde{H}_i(f)$ as explained above. Using Eq. (65) we can immediately compute the SNRs accumulated by our network

$$\bar{\rho}_h = 35.8, \quad \bar{\rho}_m = 14.3, \quad \bar{\rho}_l = 6.00. \tag{66}$$

These are comparable to actual SNRs of L1, H1, and V1 for GW170817, which are, 26.4, 18.8, and 2.0, respectively[2]. To accommodate more realistic orientations, we show two shaded regions in Fig. 1. The inspirals in the lighter region yield SNR≥ 22.34 as they sweep from 10 Hz to $f_{\text{ISCO}} \simeq 1605\,\text{Hz}$ whereas inspirals in the darker region accumulate $\bar{\rho}_l \leq$ SNR ≤ 22.34. Given a network of three equally sensitive, randomly oriented IFOs we expect that a single BNS inspiral would produce two detector strains in the darker region and one in the lighter region.

[1]Though the equations of motion for circular orbits is now known up to 4PN [16], we are not aware of any publications explicitly showing the 4PN contributions to τ_{insp} and $\mathcal{N}_{\text{cyc}}$ though we suspect that a few PN experts have already obtained these.

[2]At the time of GW170817, Virgo's sensitivity had not reached the level of LIGO's. Hence it accumulated a much smaller SNR for GW170817. By 2020, Virgo should be operating at nearly the same sensitivity of LIGO.

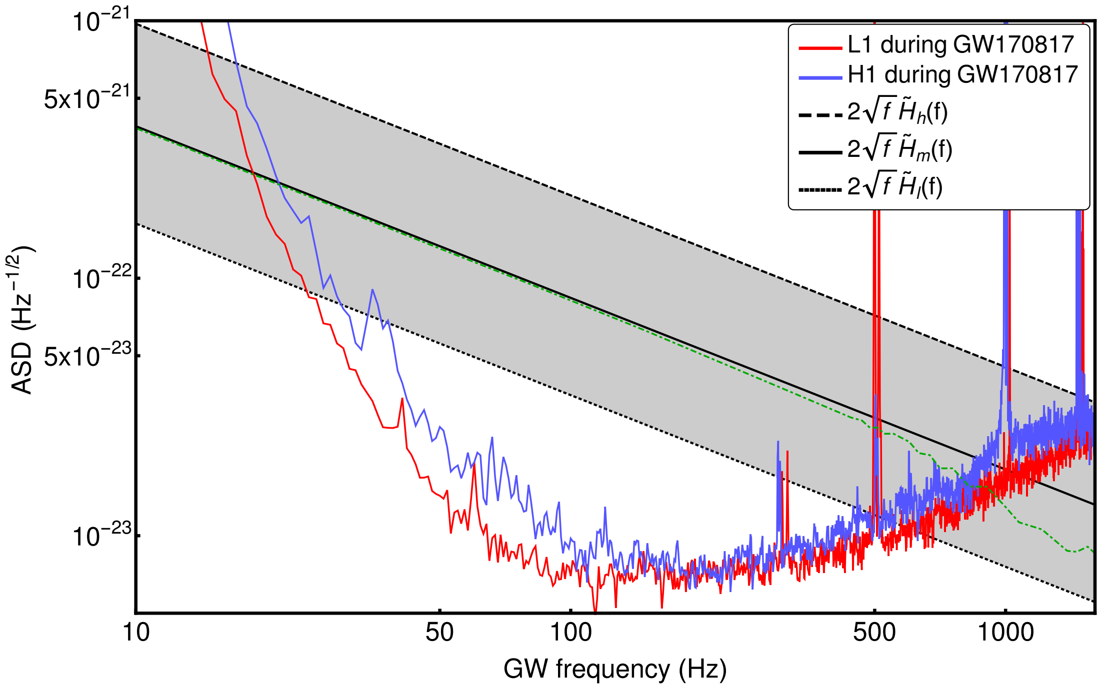

Figure 1: GW170817 as it sweeps from 10 Hz to $f_{\rm ISCO} \simeq 1605$ Hz across our network with ASD (sensitivity) of LIGO Livingstone (L1) during the event (red curve). We also show the Hanford detector's sensitivity for comparison. The dashed, solid and dotted lines represent the strains $2\sqrt{f}\tilde{H}_i(f)$ (see, e.g,. Eq. (36) and Table 1) due to the inspiral of a binary neutron star system with parameters given in Eq. (62). The change in strain amplitudes is the result of a given interferometer's orientation and the sky position of the source. In other words, the dashed line is how "loud" GW170817 is at an optimally oriented IFO with L1's sensitivity (quality factor $Q = 1$). Similarly, the solid line is the strain in a randomly oriented IFO with randomized source sky location, hence we use the RMS-averaged L1 sensitivity which effectively lowers the solid line by a factor of $2/5$. Finally, the dotted line represents a pessimistic IFO orientation and source location (sub-optimal configuration) resulting in a reduction of amplitude to 16.7% of the optimal case. The shading represents the region of likelihood for where the strain due to an inspiralling BNS would be. In the case of a three-IFO network, we expect all three strains to exist somewhere in the shaded region. The dot-dashed (green) curve shows a more realistic strain constructed with data from numerical simulations of Ref. [27]. The breakdown of the leading-order $\sqrt{f}f^{-7/6} = f^{-2/3}$ behavior around $f \sim 100$ Hz due to tidal effects is clear.

We can now compute the total SNR of GW170817 as inferred by our network

$$\bar{\rho}_{\rm tot} = \sqrt{\bar{\rho}_h^2 + \bar{\rho}_m^2 + \bar{\rho}_l^2} = 39.1\,. \tag{67}$$

This also compares well with the actual value of 32.4. Therefore, we conclude that our imaginary network performs realistically enough to make predictions on the performance of IFOs in the 2020s and 2030s.

Results: Advance warning times for inspiralling neutron stars

Our aim is to foretell GRBs using our network made up of three IFOs with A-LIGO design sensitivity in the 2020s and the Einstein Telescope sensitivity in the 2030s. Our predictive capabilities depend on how much advance warning the future networks will give us prior to the prompt merger/GRB. Our definition of advance warning is the inspiral time to the merger from a certain threshold instant $\bar{t}$ at which point the network "agrees" that there is an inspiral event statistically significant enough to issue warnings to electromagnetic telescopes. We define this threshold instant to be given at a frequency $\bar{f}$ when the total SNR equals 15. More specifically, in the case of the Advanced-LIGO-Virgo network (ALV), our statement is that there exists a frequency $\bar{f} < f_{\rm ISCO}$ such that

$$\bar{\rho}_{\rm tot} = \sqrt{\left[\rho_h(f_0^h, \bar{f})\right]^2 + \left[\rho_m(f_0^m, \bar{f})\right]^2 + \left[\rho_l(f_0^l, \bar{f})\right]^2} = 15, \tag{68}$$

where f_0^i are given by the solution set to

$$\sqrt{S_{\rm n}(f_0^i)} = 2\sqrt{f_0^i}\,\tilde{H}_i(f_0^i), \qquad i = h, m, l \tag{69}$$

with $f_0^i < \bar{f}$. In other words, f_0^i are the initial GW frequencies at which a given inspiral enters the ith IFO's sensitivity band. Once we know $\bar{f}$, we can compute the remaining time to the merger, $\tau_{\rm insp}(\bar{f})$, using Eq. (8) and its 3.5PN-enhanced version from Ref. [12]. This is what we call our advance warning time $T_{\rm AW}$. For simplicity, we set $m_1 = m_2 = 1.4M_\odot \implies M_c \simeq 1.219M_\odot$, which we justified in Point 3 of Sec. 4.3. With the masses fixed, the only variable determining h_0 is the luminosity distance D as can be seen from Eq. (37). We summarize our procedure in the flow diagram below.

Pick D	$\longrightarrow$	Construct $\tilde{H}_i(f)$	$\longrightarrow$	Compute f_0^i from Eq.(69)	$\longrightarrow$	Compute $\bar{f}$ from Eq.(68)	$\longrightarrow$	Compute $T_{AW} = \tau_{\rm insp}(\bar{f})$ from Eq. (8)

Figure 2: Flow diagram summarizing our procedure for computing advance warning times $T_{\rm AW}$ with the Advanced-LIGO-Virgo network. We will compute $T_{\rm AW}$ for the case of $M = 2.8M_\odot$ BNS system inspiralling at $D = 50, 100, 200$ Mpc.

We consider inspiralling BNS systems at $D = 50, 100, 200$ Mpc as our canonical sources for the ALV network. For each case, we compute $\bar{f}$ from Eq.(68) with which we then compute $T_{\rm AW} = \tau_{\rm insp}(\bar{f})$. We additionally calculate the total accumulated SNR from f_0 to $f_{\rm ISCO}$ for each inspiral using

$$\bar{\rho}_{\rm F} \equiv \sqrt{\left[\rho_h(f_0^h, f_{\rm ISCO})\right]^2 + \left[\rho_m(f_0^m, f_{\rm ISCO})\right]^2 + \left[\rho_l(f_0^l, f_{\rm ISCO})\right]^2}. \tag{70}$$

We will introduce the expressions for ET's $\bar{\rho}_{\rm tot}, \bar{\rho}_F$ in Sec. 6.0.2. To compute the SNRs defined above for the ALV network we require IFO noise data for which we use the ASD for the BNS-optimized A-LIGO design sensitivity expected to be attained ca. 2020 [20]. This is plotted as the thick red solid curve in Fig. 3. Sweeping across the detector's frequency bands are RMS-averaged GW strains ($\tilde{H}_m$) due to BNS inspirals at various luminosity distances. Each RMS-averaged strain is accompanied by its shaded region ranging from an optimally oriented strain ($\tilde{H}_h$) to a sub-optimally oriented strain ($\tilde{H}_l$). These regions were first explained in Sec. 5 and shown in Fig. 1. Recall that this is our way of representing the response of a three-IFO network to a single source, i.e., we map three different IFO responses due to a single source to a single IFO's response to three different sources differing in amplitudes as listed in Table 1. The height of a given strain above the detector sensitivity provides a good *visual* estimation for the corresponding SNR, but the reader should keep in mind that the actual computation involves a ratio, not a difference, as shown, e.g., in Eq. (27).

Forecasting GRBs in the 2020s with the Advanced LIGO-Virgo Network

We now compute the advance warning times that A-LIGO can provide us in the case of BNS inspirals at $D = 50, 100, 200$ Mpc. Fig. 3 displays the strains due to these inspirals in the same fashion as Fig. 1: the solid (black), dotted (blue), and dashed (green) lines represent the RMS-averaged characteristic strains, $2\sqrt{f}\tilde{H}_m(f)$, at luminosity distances of $D = 50, 100, 200$ Mpc, respectively, with the shaded regions covering the range between the optimally oriented case and the sub-optimal case.

The computation follows the procedure outlined in Fig. 2. We use numerical root finding to determine $\bar{f}$ and f_0^i for all three values of D. The computation of SNRs and advance warning times is straightforward. We summarize our results in Table 3 where we present both the 0PN and the 3.5PN results for the advance warning times $T_{\rm AW}$. As can be seen from the values for $T_{\rm AW}$ in the table, we can at best expect 100 seconds of early warning time. This time increases to 2.5 minutes in the case of another GW170817-like event with $D = 40$ Mpc. The current best estimate for the event rate of BNS

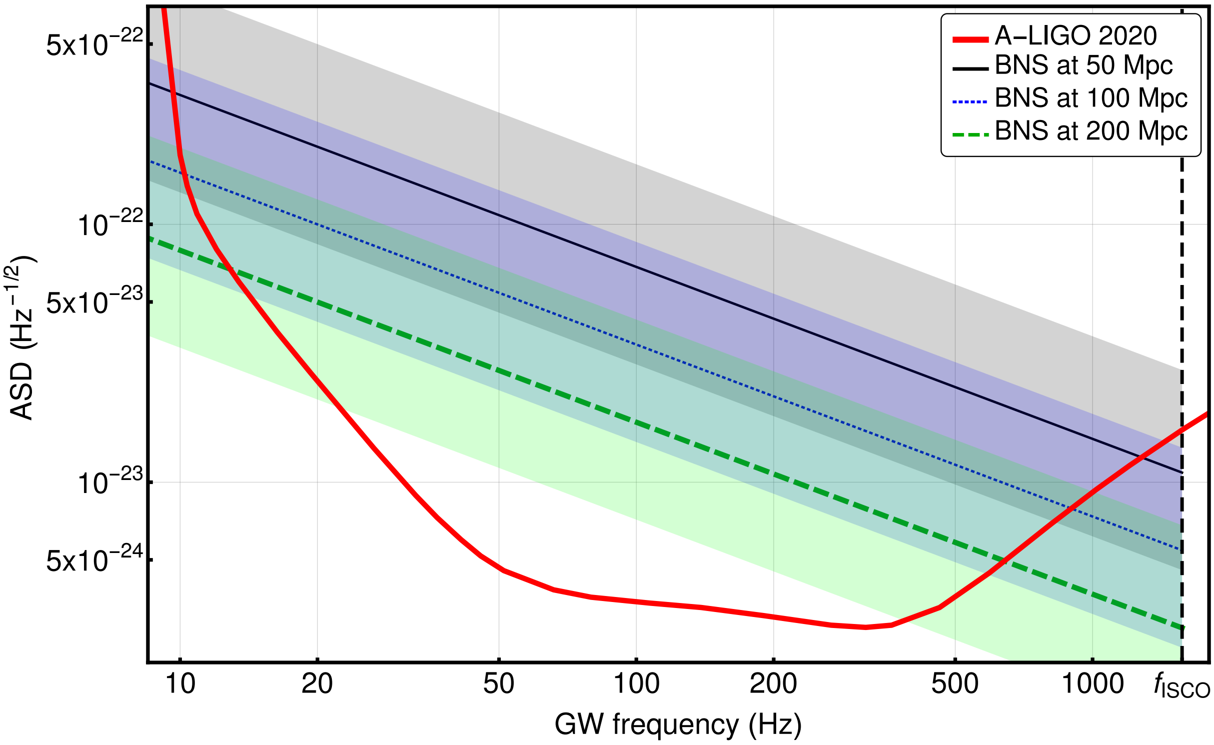

Figure 3: Typical $M = 2.8 M_\odot$ BNS inspirals sweeping across the Advanced LIGO-Virgo network in the 2020s. These may be the harbingers of short GRBs. The solid (black), dotted (blue), and dashed (green) lines are the RMS-averaged strains ($2\sqrt{f}\tilde{H}_m(f)$) at luminosity distances of $D = 50, 100, 200\,$Mpc, respectively. The accompanying shaded regions cover the region of likelihood for a three-IFO network as explained in Fig. 1. The vertical dashed (black) line marks the ISCO frequency $f_{\rm ISCO} \simeq 1571\,$Hz at which point we terminate the inspirals, but as can be seen, the SNR hardly increases beyond $\sim 1000\,$Hz.

inspirals is $1540^{+3200}_{-1220}\,\mathrm{Gpc}^{-3}\mathrm{yr}^{-1}$, inferred from the O1 and O2 observing periods of Advanced LIGO [8]. This translates to ≈ 0.1 event per (40-Mpc)^3 per year, or taking the upper limit ≈ 0.3. So we can at best hope to detect one 40-Mpc inspiral per three years or longer. Therefore, we do not expect to be able forecast GRBs in the Advance LIGO-Virgo era given that we might at best have a couple of minutes of warning time. However, given Moore's law and new search approaches based on deep learning ([33]) we prefer to remain optimistic about the prospects of forecasting at least one GRB in the 2020s.

D (Mpc)	$\bar{f}$ (Hz)	$T_{\rm AW}^{0PN}$(sec)	$T_{\rm AW}^{3.5PN}$(sec)	$\bar{\rho}_F$
50	22.8	111.1	113.1	84.2
100	36.2	32.41	33.08	42.1
200	79.3	4.859	4.948	21.0

Table 3: The Advanced LIGO-Virgo (ALV) network's potential for providing advance warning times, $T_{\rm AW}$, to electromagnetic observatories for inspiralling binary neutron stars at luminosity distances of $D = 50, 100, 200\,$Mpc. $\bar{f}$ is the frequency at which the signal-to-noise ratio (SNR) accumulated by the ALV network reaches 15. $\bar{\rho}_F$ is the total accumulated network SNR for each inspiral. We present both the Newtonian (0PN) and the 3.5 post-Newtonian result for the advance warning times.

In addition to potentially alerting the E & M community, the ALV network will accumulate impressive SNRs (see $\bar{\rho}_F$ in Table 3) for BNS inspirals out to $100\,$Mpc. Monte-Carlo simulations of BNS systems indicate that the measurement errors for the system parameters are proportional to $\bar{\rho}_F^{-1}$ [24]. Therefore, systems that yield high SNRs ($\bar{\rho}_F \gtrsim 40$) will enable (i) high precision measurements of M_c, M [25]; (ii) sky localization to $\lesssim 5\,\mathrm{Deg}^2$ [26]; (iii) $\lesssim 10\%$ precision in the inferred NS masses [26] and the effective spin parameter $\chi_{\rm eff}$ [31]; and (iv) restrictions on the equation of state and the tidal deformability parameters of neutron stars [27, 28, 29, 30]. We should caution the reader that such systems will make up $\lesssim 1\%$ of the population of BNSs detected by the ALV network [36].

Forecasting GRBs in the 2030s using the Einstein Telescope

We now wish to quantify the forecasting capabilities of Einstein Telescope. To this end, we consider the inspiral of BNS systems at luminosity distances of $100, 200, 400, 1000\,$Mpc entering the ET band. The SNR accumulated at ET by each inspiral is given by a slight modification to Eq. (47)

$$\bar{\rho}_{\rm tot,ET} = \frac{36}{25} A^2 h_0^2 \int_{f_0}^{f_{\rm ISCO}} df \, \frac{f^{-7/3}}{S_n(f)}, \tag{71}$$

where f_0 is the GW frequency at which the emitted GWs enter ET's detection band, i.e, $f_0 < f_{\rm ISCO}$ such that

$$\sqrt{S_{\rm n}(f_0)} = 2\sqrt{f_0}\,\tilde{H}_{\triangle}(f_0, D) \tag{72}$$

with $\tilde{H}_{\triangle}(f, D)$ given by Eq. (48). For the detector noise $\sqrt{S_n(f)}$, we adopt the ASD for the B and C configurations known as ET-B and ET-C, respectively [21] which we plot as the solid dark (red) and light (brown) curves in Fig. 4. Sweeping across these are four BNS inspirals at $D = 100, 200, 400, 1000\,$Mpc represented by solid (black), dotted (blue), dashed (green), and dot-dashed lines (gray), respectively. These strains sit much higher than the detector noise comparred with those in Fig. 3 which foretells us that the SNRs in the ET band will be much higher, thus the resulting advance warning times will be much longer.

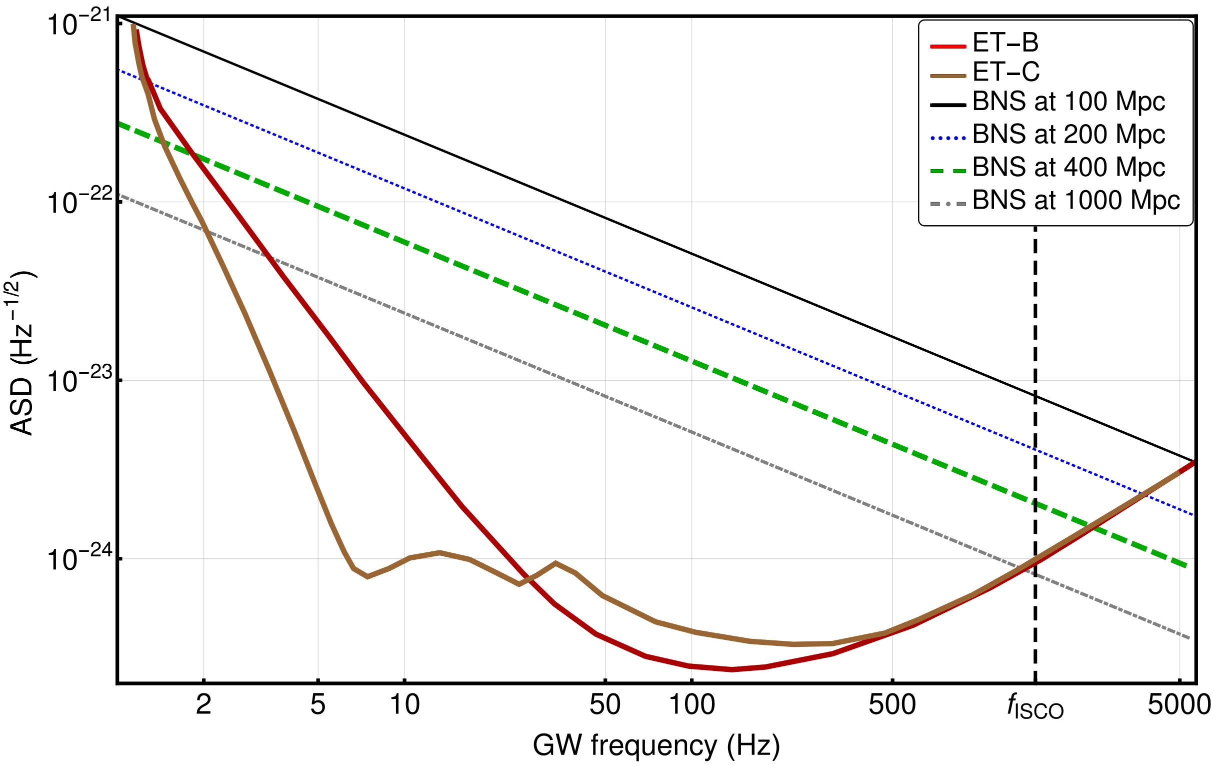

Figure 4: Typical GW sources that may be harbingers of GRBs in the 2030s: $M = 2.8M_\odot$ inspiralling BNS systems sweeping across the Einstein Telescope's sensitivity band for both B and C configurations. The solid (black), dotted (blue), dashed (green), and dot-dashed lines (gray) lines are the RMS-averaged strains, $2\sqrt{f}\tilde{H}_{\triangle}(f, D)$, at luminosity distances of $D = 100, 200, 400, 1000\,$Mpc, respectively. The vertical dashed (black) line marks $f_{\rm ISCO} \simeq 1571\,$Hz at which point we terminate the inspirals, but numerical simulations indicate that the actual ISCO is smaller than the Schwarzschild value $6GM/c^2$ hence the true ISCO frequency is greater than $f_{\rm ISCO}$ used here. As the plot shows, Einstein Telescope is sensitive enough in this regime to accumulate more SNR.

To determine $T_{\rm AW}$ we once again impose the threshold SNR of 15 which is our criterion for sending out warnings to electromagnetic observatories. Thus, rewriting Eq. (68) in the case of ET, we define $\bar{f}_{\rm ET}$ as the solution to

$$15 = \frac{36}{25} A^2 h_0^2 \int_{\bar{f}_{\rm ET}}^{f_{\rm ISCO}} df \, \frac{f^{-7/3}}{S_n(f)}. \tag{73}$$

This gives us our advance warning time $T_{\rm AW} = \tau_{\rm insp}(\bar{f}_{\rm ET})$ using Eq. (8) which we can slightly improve by using the 3.5PN expression. Therefore we will proceed in a manner similar to the procedure summarized in Fig. 2) and compute the 0PN and 3.5PN advance warning times for all four inspirals in both the ET-B and ET-C bands. We define the final accumulated SNR as

$$\bar{\rho}_{F,\,\rm ET} \equiv \frac{36}{25} A^2 h_0^2 \int_{f_0}^{f_{\rm ISCO}} df \, \frac{f^{-7/3}}{S_n(f)}. \tag{74}$$

D (Mpc)	$\bar{f}$ (Hz)	$T_{\rm AW}^{0PN}$(sec)	$T_{\rm AW}^{3.5PN}$(sec)	$\bar{\rho}_{F,\,\rm ET}$
100	1.1435	2909	2942	307.1
200				

Table 4: ET-B

Binary black hole neutron star systems

Tidal disruption, minimum BH mass $5M_{\odot}$. Tidal force $\sim M/r^3 \sim M^{-2}$ hence the smaller the BH the more TD there will be. Also need highly spinning BH to decreases the ISCO radius.

References

[1]

[2] `http://gwcenter.icrr.u-tokyo.ac.jp/en/`

[3] Akutsu et al. see bibtex

[4]

[5] https://arxiv.org/pdf/1607.08697.pdf

[6] 1603.02698 [astro-ph.HE]

[7] The Astrophysical Journal, Volume 675, Issue 1, article id. 670-682, pp. (2008)., arXiv:0711.0925.

[8]

[9]

[10] 1610.05309 [astro-h.HE]

[11]

[12]

[13] J. W. T. Hessels, S. M. Ransom, I. H. Stairs, P. C. C. Freire, V. M. Kaspi, and F. Camilo, Science 311, 1901 (2006).

[14] Schutz, Satyaprakash, LRR

[15] GW170817 Factsheet `https://www.ligo.org/detections/GW170817/images-GW170817/GW170817_Factsheet.pdf`.

[16] L. Bernard et al., [gr-qc:1711.00283]

[17] J. Reid, the NS inspiral figure tidal corrections

[18] Data release for GW170817 `https://losc.ligo.org/events/GW170817/`

[19] LIGO Open Science Center signal processing tutorial at `https://losc.ligo.org/s/events/GW150914/GW150914_tutorial.html`

[20] Advanced LIGO anticipated sensitivity curves at `https://dcc.ligo.org/LIGO-T0900288/public`

[21] S. Hild et al. Class.Quant.Grav. 28 (2011) 094013 arXiv:1012.0908 [gr-qc] (see bixtex below)

[22] LSST

[23] ApJ paper

[24]

[25]

[26]

[27]

[28]

[29]

[30]

[31]

[32]

[33]

[34]

[35]

[36]

[37]